Magnetic and structural properties of Fe-implanted cubic GaN

V. A. N. Righetti, X. Gratens, V. A. Chitta, M. P. F. de Godoy, A. D. Rodrigues, E. Abramof, J. F. Dias, D. Schikora, D. J. As, and K. Lischka

---

Articles you may be interested in

Structural, optical, and magnetic properties of highly-resistive Sm-implanted GaN thin films
J. Appl. Phys. **116**, 043909 (2014); 10.1063/1.4891226

Structural and magnetic properties in Mn-doped GaN grown by metal organic chemical vapor deposition
Appl. Phys. Lett. **92**, 152116 (2008); 10.1063/1.2909545

Magnetic and structural properties of Gd-implanted zinc-blende GaN
Appl. Phys. Lett. **90**, 262505 (2007); 10.1063/1.2753113

Room temperature ferromagnetism in cubic GaN epilayers implanted with Mn + ions
Appl. Phys. Lett. **85**, 3777 (2004); 10.1063/1.1812590

Magnetic and structural properties of Co, Cr, V ion-implanted GaN
J. Appl. Phys. **93**, 4512 (2003); 10.1063/1.1561587

Magnetic and structural properties of Fe-implanted cubic GaN

V. A. N. Righetti,[1] X. Gratens,[1] V. A. Chitta,[1] M. P. F. de Godoy,[2] A. D. Rodrigues,[2]
E. Abramof,[3] J. F. Dias,[4] D. Schikora,[5] D. J. As,[5] and K. Lischka[5]

[1]*Instituto de Física, Universidade de São Paulo, 05315-970 São Paulo, Brazil*
[2]*Departamento de Física, Universidade Federal de São Carlos, 13565-905 São Carlos, Brazil*
[3]*LAS, Instituto Nacional de Pesquisas Espaciais, 12245-970 São José dos Campos, Brazil*
[4]*Instituto de Física, Universidade Federal do Rio Grande do Sul, 91501-970 Porto Alegre, Brazil*
[5]*Universität Paderborn, 133098 Paderborn, Germany*

In this article, we report on structural and magnetic properties of cubic GaN epitaxial layers implanted with Fe ions and subsequently subjected to thermal annealing. The epitaxial quality of the layers was studied by X-ray diffraction rocking curves (ω-scans) and Raman spectroscopy. The results show that the implantation damages the crystal structure producing an expansion of the lattice parameter in the implanted region. These damages are partially removed by the thermal treatment. Room temperature ferromagnetism is observed for the sample implanted with a dose of $1.2 \times 10^{16} \, cm^{-2}$, while samples implanted with $2.4 \times 10^{16} \, cm^{-2}$ show a coexistence of ferromagnetism and paramagnetism due to disperse Fe^{3+}. Thermal annealing changes these magnetic properties. For the low dose sample, the ferromagnetism is converted into paramagnetism while for the high dose we observed an enhancement of the ferromagnetic contribution characterized by a superparamagnetism behavior attributed to Fe-based particles. *Published by AIP Publishing.*
[http://dx.doi.org/10.1063/1.4962275]

I. INTRODUCTION

Diluted magnetic semiconductor (DMS) based on wide band gap GaN compound doped with manganese ions has attracted attention as a possible high Curie temperature (T_C) spintronic material.[1] Another potential candidate for spintronic application is GaN doped with iron ions. A recent theoretical work[2] predicts positive *p-d* exchange integrals for Fe^{3+} doped GaN, indicating ferromagnetic interaction between Fe ions. Experimentally, ferromagnetic behavior has been observed in a *p*-type GaN layer implanted with Fe ions.[3,4] Both results were obtained for stable hexagonal (*h*) GaN phase. From our knowledge, studies on metastable cubic (zincblende) GaN implanted Fe ions have not been reported yet. Cubic (*c*) GaN phase exhibits different properties compared to the *h* phase: higher symmetry of the lattice, absence of spontaneous polarization effects, resulting in higher mobilities and smaller effective masses.[5] Implantation studies in *c*-GaN have been performed with Eu,[6] Mn,[7] and Gd[8] ions and revealed different results compared to the corresponding *h*-GaN implanted samples. In this paper, we report on the properties of cubic GaN layers implanted with Fe ions. The cubic GaN epitaxial layers have been grown on a 3C-SiC substrate. 3C-SiC can be useful as an intermediate layer or a substrate for cubic GaN growth, since the lattice mismatch between SiC and GaN is only 3.5%. Results of structural and magnetic investigations are presented for as grown, as implanted and annealed samples. Room temperature ferromagnetism has been observed in the samples.

II. EXPERIMENTAL

A set of three cubic GaN layers with a thickness of about 0.8 μm were grown directly on (001) oriented 3C-SiC 200 μm thick substrate by plasma assisted molecular beam epitaxy (PA-MBE). The growth process was controlled by *in situ* reflection high-energy electron diffraction (RHEED). Details of the growth process can be found in Ref. 9. Each layer was cut into 2 pieces of about the same size ($\simeq 5 \times 5 \, mm^2$). One piece was kept unimplanted to be used as a reference. The other piece was implanted at room temperature. The implantation was carried out using an ion beam energy of 200 keV. Two different doses of Fe ions of $1.2 \times 10^{16} \, cm^{-2}$ and $2.4 \times 10^{16} \, cm^{-2}$ have been used. The sample with the lowest dose and its associated reference are labeled as sample Fe1I and Ref1, respectively. For the largest dose, two samples from different layers have been implanted. They are labeled as samples (associated references) Fe2aI (Ref2a) and Fe2bI (Ref2b), respectively. Based on the implantation conditions, simulations using SRIM (Stopping and Range of Ions in Matter)[10,11] predict a roughly Gaussian implantation profile centered at 90 nm from the surface with a Fe atomic concentration (% atomic) at the peak profile of 1.2% and 2.4% for the lowest and highest doses, respectively.

After implantation, the samples were annealed under nitrogen atmosphere with a nonimplanted GaN layer placed face to face on the top of the implanted layer. This procedure was used to prevent evaporation of nitrogen near the surface and possible incorporation of impurities. The heat treatment was performed at 900 °C for 5 min. After this procedure, the samples are labeled Fe1A, Fe2aA, and Fe2bA.

The crystalline quality of the GaN layer after growth, implantation and heat treatment was inspected by X-ray diffraction (XRD) in the Bragg-Brentano configuration (Cu$K\alpha_1$ and Cu$K\alpha_2$) and by high-resolution X-ray diffraction (HRXRD) (Cu$K\alpha_1$). The structural characterization was completed with non-polarized Raman spectroscopy in a

backscattering configuration at room temperature using a 568 nm laser excitation. There, the incoming and scattered radiation propagate perpendicularly to the layer, i.e., along the (001) axis of the 3C-SiC substrate. The magnetic properties of the samples were investigated using a Cryogenic S600 superconducting quantum interference device (SQUID) with high sensitivity, of about 10^{-7} emu, from 1.7 K to 300 K with the magnetic field applied parallel to the layer plane.

III. RESULTS AND DISCUSSION

A. Crystalline quality

Figure 1 shows the XRD pattern obtained for sample Ref1. The displayed spectrum is similar to the obtained for the as implanted and as annealed samples. The scale on the x-axis includes a break for a better view of the relevant features of the spectrum (in the interval break, there are no relevant reflections). Besides the main peaks of the 3C-SiC (001) substrate ((002) and (004) reflections at 41.4° and 90°, respectively[12]), the XRD pattern shows two peaks due to the cubic GaN (001) layer. The sharp and intense peak at $2\theta = 40.03°$ corresponds to the (002) reflection. The broad peak at about $2\theta = 86.5°$ is due to the (004) plane of c-GaN. There are no other reflections corresponding to cubic GaN, indicating that the GaN epilayer is strongly aligned to the substrate. Using both values of the diffraction angles, we may determine the lattice parameter $a = 4.505 \pm 0.002$ Å for the present cubic GaN epilayer. This result is in good agreement with previous works.[13–15]

In addition to the cubic material reflections (3C-SiC and GaN), two other peaks, with low intensity, can be observed near $2\theta = 37.25°$ and $2\theta = 79.35°$. These peaks cannot be ascribed to the cubic GaN layer. It is well established that, due to its metastable nature, a pure zincblende GaN phase is difficult to grow without the appearance of small inclusions of a wurtzite GaN phase.[16–18] The two subsidiary peaks were then tentatively attributed to reflections from hexagonal GaN. Based on the bulk values of the lattice parameters for h-GaN, $a = 3.1879$ Å and $c = 5.1856$ Å,[19] peaks at $2\theta = 37.25°$ and $2\theta = 79.35°$ can be ascribed to the reflection of the wurtzite

plane $(10\bar{1}1)$ and $(20\bar{2}2)$, respectively. Both reflections show small deviations from the expected positions for bulk h-GaN, which may indicate a stressed hexagonal phase. As shown in Figure 1, reflection of the hexagonal (0002) plane is absent in the XRD pattern. The result shows that the hexagonal $(10\bar{1}1)$ planes are closed in orientation to the cubic (001) plane. From the ratio of the integrated intensity between the (002) and $(10\bar{1}1)$ peaks, more than 98.5% of the GaN layer was found to be cubic.

As mentioned above, no changes in the XRD pattern, presented in Figure 1, have been observed for the implanted and annealed samples. Magnetic secondary phases such as metallic Fe or iron nitrides were not detected. However, due to the insensitivity of XRD to nanoscale precipitates,[20] the existence of such magnetic secondary phases cannot be completely ruled out.

More detailed information about the effect of implantation and thermal treatment on the crystalline quality of the GaN layers were obtained from HRXRD measurements. Figure 2 shows the rocking curves of the (002) cubic GaN reflection taken for sample Fe2aI and after annealing at 900 °C (Fe2aA). The curve obtained for virgin sample Ref2a is also displayed. The full width at half maximum (FWHM) of the (002) GaN peak is 23 arc min for the as grown sample Ref2a. This value is smaller than or similar to previous reports (FWHM = 28 arc min in Ref. 21, 60 arc min in Ref. 22, and
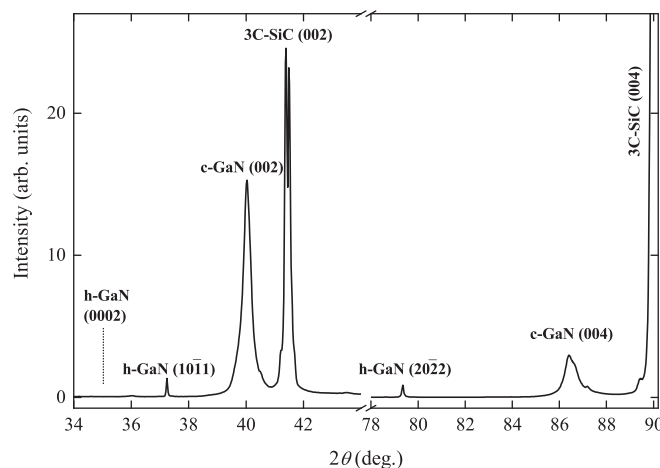

FIG. 1. Relevant part of the XRD pattern of a GaN epitaxial film grown on (001) 3C-SiC substrate. The displayed pattern is typical for all studied samples.
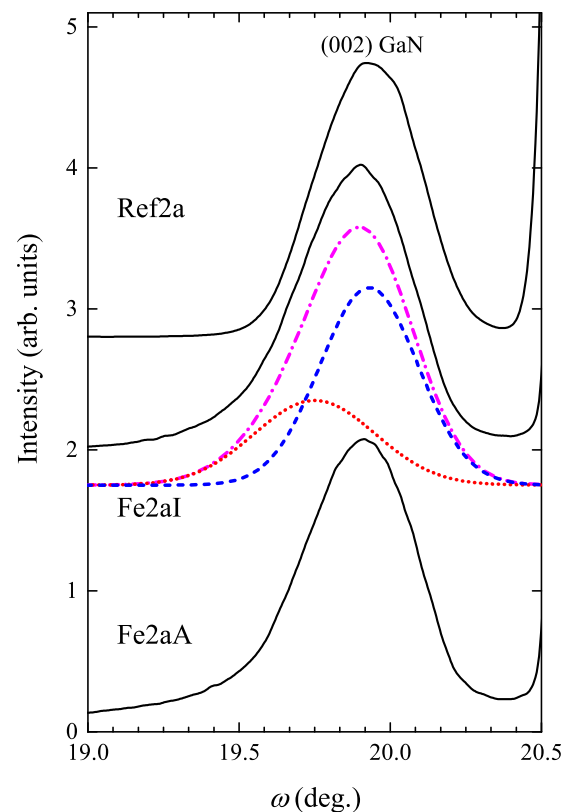

FIG. 2. X-Ray rocking curve of the cubic (002) GaN diffraction peak obtained for the as implanted layer (Fe2aI) and for the same layer after annealing (Fe2aA). Data obtained for the as grown sample Ref2a are also displayed. A vertical shift is included for a better view. The dotted-dashed line (in pink) is the result of a simulation of the asymmetric broadening of the peak observed after implantation. This line is a superposition of two peaks, one shown as a dotted line (in red) and the other as a dashed line (in blue).

96 arc min in Ref. 15). Okumura *et al.*[23] have reported a rocking curve FWHM of 16 arc min for cubic GaN grown by MBE on the 3C-SiC substrate. Based on this last result, we may consider that our cubic GaN layers have a very good structural quality.

After implantation, we observe a broadening of the (002) diffraction peak with FWHM = 26.8 arc min. The broadening is found to be asymmetric with a tail extended to small angles (to the left of the peak). The observed broadening can be simulated using two peaks as shown in Figure 2. The main peak (dashed line) is attributed to the nonimplanted region of the layer and is modeled using the position and the FWHM obtained for sample Ref2a. The relative intensity, position, and linewidth of the second peak, in dotted line, were then adjusted in order to give a good match between the simulation and the experimental results. This peak is ascribed to the implanted region of the layer, where the Fe implantation causes an expansion of the lattice parameter. The same kind of effect has been observed in previous works.[6,8,24–26]

After annealing at 900 °C, the FWHM value is found to be 25.9 arc min. This small decrease, compared to the implanted sample, indicates a partial diffusion of the Fe ions from the implanted to the nonimplanted region of the layer. The observed features for sample Fe2aI are not present in sample Fe1I (low dose). In this case, no changes in the rocking curve have been observed after implantation and after annealing.

Figure 3 shows the Raman spectra taken at room temperature and in backscattering configuration of the as grown (Ref2a), as implanted (Fe2aI) and as annealed after implantation (Fe2aA) samples. In the case of the as grown sample, two strong Raman peaks are observed, one around 797 cm^{-1}

that is ascribed to the transversal optical (TO) phonon peak of the 3C-SiC substrate and another around 737 cm^{-1} assigned to the longitudinal optical (LO) phonon peak of the *c*-GaN layer. In addition, a structure of two peaks centered around 560 cm^{-1} can be observed. The structure is composed of a sharp peak at 566 cm^{-1}, ascribed to the high frequency E2 mode of the *h*-GaN, and a broad peak at 555 cm^{-1}, ascribed to the TO mode of the *c*-GaN layer. The present identification of the Raman peaks has been performed based on previous results.[27,28] In the backscattering configuration and for a perfect crystal, the LO component of the *c*-GaN and the E2 modes of the *h*-GaN are Raman allowed, while the TO component for the *c*-GaN is Raman forbidden. As described in Ref. 28, the experimental observation of the TO mode of the *c*-GaN can be attributed to a lack of crystalline quality of the epitaxial layer, and the intensity ratio (I_{TO}/I_{LO}) between the TO and LO peaks can be used to test it. For sample Ref2a, we have estimated $I_{TO}/I_{LO} = 0.1$. As shown in Figure 3(b), the implantation process strongly reduced the intensity of the Raman spectra. The observed feature is attributed to the layer amorphization in the implanted region. Raman spectra taken after thermal annealing are characterized by the regain of the LO *c*-GaN peak, which confirms a partial recover of the original crystalline quality. It can be noted also a strong reduction of the intensity of the two peaks centered around 560 cm^{-1}.

B. Magnetic properties

Preliminary measurements (Figure 4) show that the reference samples (the GaN layer on the SiC substrate) exhibit a linear variation of the magnetization (*M*) as a function of magnetic field (*H*). From these data, we have determined the diamagnetic constant $\chi_d = (-2.6 \pm 0.2) \times 10^{-7}$ emu/g. This value agrees well with the diamagnetic constant of cubic SiC $\chi_d = -2.67 \times 10^{-7}$ emu/g.[12]

Figure 5 displays the *M* vs. *H* data taken for the three as implanted samples at $T = 300$ K and 10 K. Here, *M* is calculated using the overall mass of the sample (layer and substrate) in order to detect any change compared to reference samples. For all curves the diamagnetic contribution from the substrate can be noted. In addition, Fe1I sample exhibits
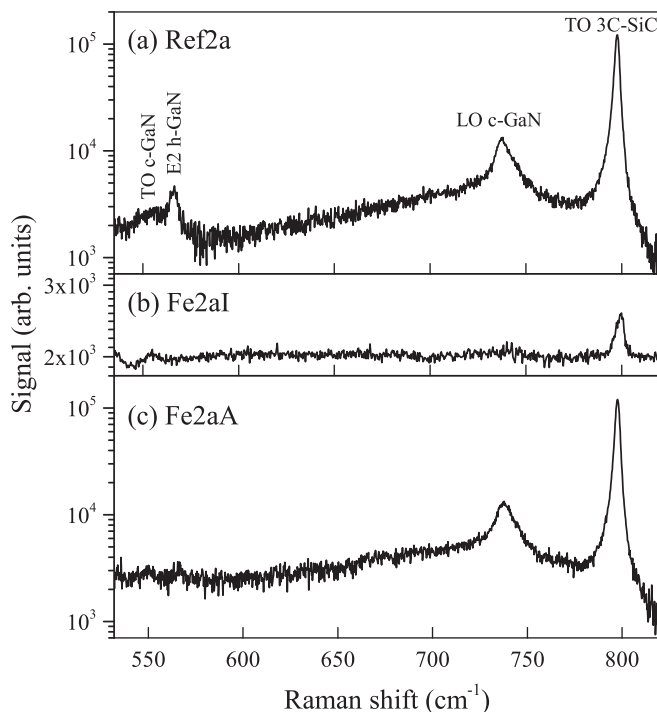

FIG. 3. Non-polarized room-temperature Raman spectra of the as grown Ref2a (a), as implanted Fe2aI (b), and annealed Fe2aA (c) samples.
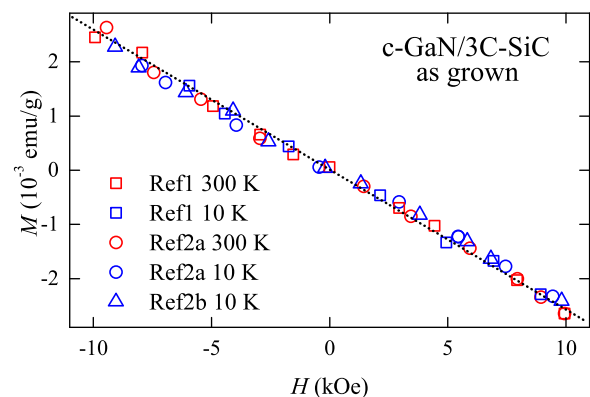

FIG. 4. Magnetization data at $T = 300$ K and 10 K for the three *c*-GaN/3C-SiC reference samples. Only few data for each sample have been plotted for clarity. The dotted line represents a linear variation of *M* vs. *H* which correspond to a diamagnetic contribution with $\chi_d = -2.6 \times 10^{-7}$ emu/g.
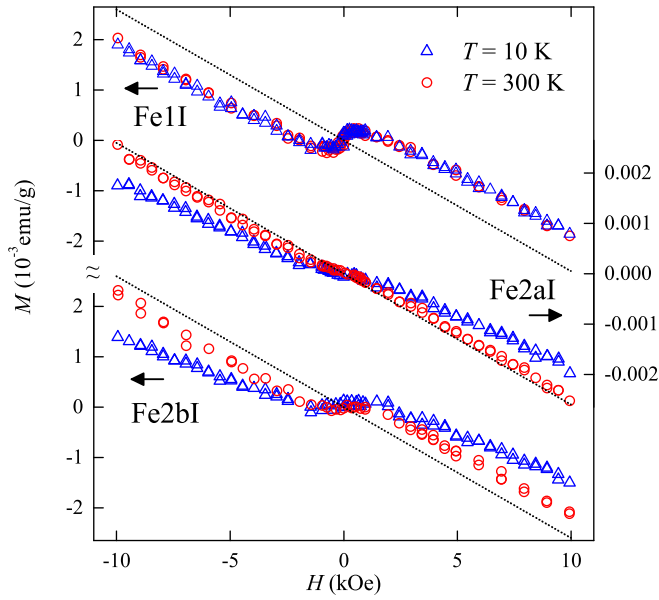
FIG. 5. Magnetization curves for the as implanted Fe1I, Fe2aI, and Fe2bI samples obtained at $T = 10$ K and 300 K. The dotted line represents the diamagnetic contribution from the substrate. Arrows indicate the magnetization scale for each sample.

a clear room temperature ferromagnetic characteristic. The magnetization saturation (M_S) value is found to be T-independent with $M_S = 5.6 \times 10^{-4}$ emu/g. For sample Fe2aI, ferromagnetism is not observed, but we may note a significant increase of the slope of the M vs. H curve when T is lowered to 10 K, which indicates the existence of a paramagnetic contribution. Finally, data from sample Fe2bI show features of paramagnetic and ferromagnetic contributions. For this sample, the ferromagnetic contribution is also T-independent with $M_S = 4.4 \times 10^{-4}$ emu/g.

The presence of a paramagnetic contribution is more evident for samples Fe2aI and Fe2bI when we explore the DC susceptibility χ vs. T curves displayed in Figure 6. For
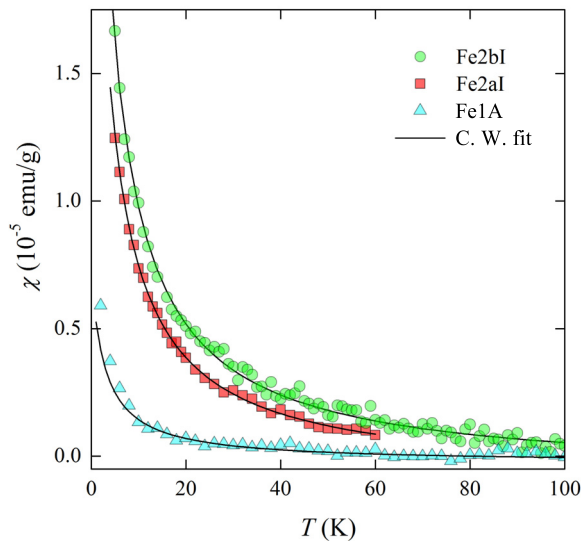

FIG. 6. Magnetic susceptibility vs. temperature data of the paramagnetic Fe^{3+} contribution observed in as-implanted Fe2aI and Fe2bI and postannealed Fe1A GaN layers. The symbols represent experimental data, while lines are the best fit to the Curie-Weiss law.

sample Fe2aI (which shows only a paramagnetic phase), data were obtained by measuring the magnetization at low magnetic fields ($\chi = M/H$). For sample Fe2bI, due to the existence of a ferromagnetic contribution, the χ vs. T data of the paramagnetic contribution were obtained by measuring the magnetization for selected values of H (well above the saturation of the ferromagnetic contribution) for each value of T. The magnetic susceptibility is then given by the slope $\frac{\Delta M}{\Delta H}$ of the obtained data. In Figure 6, the data have been corrected to the diamagnetic contribution from the substrate and χ is displayed in emu per gram of the GaN layer.

As shown in Figure 6, the χ vs. T traces are well fitted by the Curie-Weiss law. The values of the Curie constant C determined by the fit are given in Table I. A Curie-Weiss temperature $\theta = (-1.0 \pm 0.1)$ K is obtained for both Fe2aI and Fe2bI samples.

Thermal annealing results in significant changes in the magnetic properties of the implanted layers. The ferromagnetic contribution observed for the as-implanted sample (Fe1I) disappears after annealing (sample Fe1A). In addition, we observe the appearance of a paramagnetic contribution (Figure 6) which can be characterized by the Curie constant given in Table I and the Curie-Weiss temperature $\theta = (-0.5 \pm 0.1)$ K. For both Fe2aA and Fe2bA samples, the paramagnetic contribution is found to be unchanged after annealing. Fit of χ vs. T traces with the Curie-Weiss law gives similar values (within experimental errors) of the Curie constant for pre and postannealed samples. The change in the Fe2aA sample is characterized by the appearance of a ferromagnetic contribution observed at room temperature (Figure 7), while for Fe2bA by an enhancement of the existing postimplanted ferromagnetism. For both samples, the M_S values at $T = 300$ K are given in Table I. In addition, the observed postannealing ferromagnetic contribution exhibits different features compared to the postimplanted samples. In Figure 7, we observe an increase of the value of M_S for decreasing T. The variation of M_S as a function of T can be also observed in Figure 8. There, M_S has been obtained by extrapolating the linear part of the M vs. H traces to zero field. The symbols represent M_S obtained from curves as in Figure 7, while the dotted line represents data obtained for a set of few selected magnetic field values only. The increase of M_S is clearly observed for a decrease of T down to 30 K. Below 30 K the paramagnetic contribution difficult the observation of any variation in M_S. For $T = 1.7$ K, the overall magnetization can be simulated by a Brillouin function for the paramagnetic phase plus the ferromagnetic contribution obtained at $T = 30$ K.

From the SRIM simulation, the density of Fe ions considering the overall volume of the GaN layer was determined to be $N_{SRIM} = 2.06 \times 10^{20}$ cm^{-3} for the higher dose and one half of it for the lower dose. Assuming here that all the observed magnetic contributions are due to Fe^{3+} ions, we may determine its effective concentration within the samples using the obtained values of M_S and C. From the magnetization saturation of the ferromagnetic contribution, the Fe^{3+} concentration is given by $N_{Fe^{3+}} = M_S/g\mu_B S$ and from the Curie constant we have $N_{Fe^{3+}} = 3k_B C/g^2\mu_B^2 S(S + 1)$,

TABLE I. Magnetic parameters determined for the implanted and implanted/annealed samples. M_S is the magnetization saturation value of the ferromagnetic (F) contribution. C is the Curie constant of the paramagnetic contribution (P). M_S is found to be independent of temperature for the implanted samples while, for the postannealed samples, M_S depends on the temperature, and the displayed values are for $T = 300$ K. M_S and C are expressed in emu/g and emu K/g of the GaN layer. IR is the implantation ratio given by $N_{Fe^{3+}}/N_{SRIM}$ (see Text).

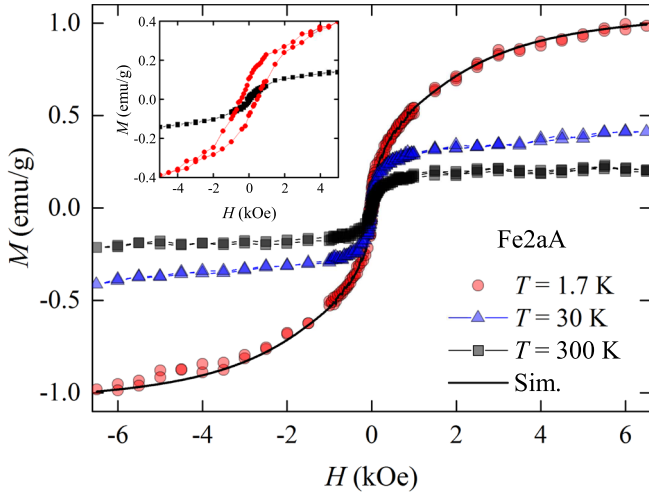| Sample		After implantation					After annealing			
		$M_S \times 10^2$	IR (%)	$C \times 10^5$	IR (%)		$M_S \times 10^2$	IR (%)	$C \times 10^5$	IR (%)
Fe1	F	7.3 ± 0.1	≈ 10	…	…	P	…		1.5 ± 0.5	≈ 12
Fe2a	P	…	…	7.8 ± 0.5	≈ 30	F-P	17.8 ± 0.1	≈ 11	7.8 ± 0.5	≈ 30
Fe2b	F-P	5.8 ± 0.1	≈ 4	10.0 ± 0.5	≈ 40	F-P	12.6 ± 0.1	≈ 8	10.0 ± 0.5	≈ 40

FIG. 7. M vs. H curves obtained for the postannealed Fe2aA sample at $T = 300$ K, 30 K, and 1.7 K. The diamagnetic contribution from the substrate has been subtracted. The line represents a simulation of the data at 1.7 K using a Brillouin function plus the ferromagnetic contribution obtained at 30 K.
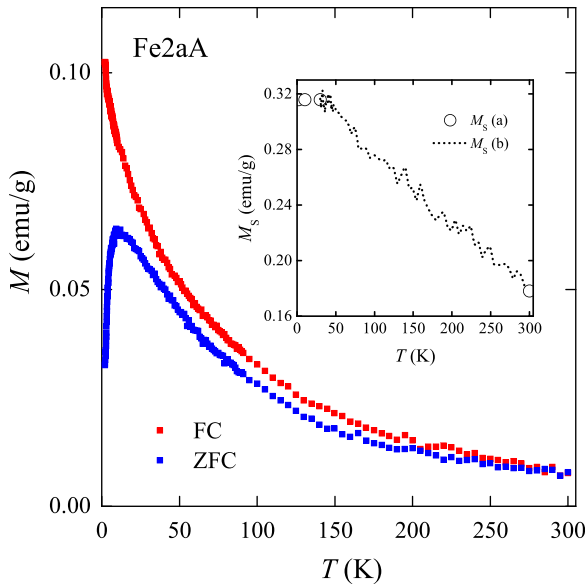

FIG. 8. Zero field cooling and field cooling magnetization vs. temperature curves for the postannealed Fe2aA layer obtained for $H = 500$ Oe. Data have been corrected to the diamagnetic contribution from the substrate as well as to the Curie-Weiss like magnetization of the paramagnetic contribution. The inset shows the magnetization saturation value of the ferromagnetic contribution as a function of temperature. Data were obtained from extrapolation of the linear part of the M vs. H curves to zero field. (a) Data like in Figure 7 have been used. (b) Data obtained from traces with few values of the magnetic field have been used.

where g is the Landé factor ($g = 2$), μ_B is the Bohr magneton, S is the spin ($S = 5/2$), and k_B is the Boltzmann constant. For the Fe2bI sample with $M_S = 5.8 \times 10^{-2}$ emu/cm^3 (Table I), we obtain $N_{Fe^{3+}} = 7.75 \times 10^{18}$ cm^{-3}, which correspond to an implantation ratio (IR) of $N_{Fe^{3+}}/N_{SRIM} = 3.7\%$. The IR values determined for the other samples (postimplanted and postannealed) are given in Table I.

The results point out to a low efficiency of the implantation process. The maximum implantation ratio is observed for the Fe2bA sample with a total of 43% of effectively implanted Fe ions. Weak efficiency of the implantation has been also observed in a previous work on Mn implanted GaN sample where only 7% of the Mn dose contributed to the M_S value.[7] A possible explanation for the weak effective implanted concentration may be the coexistence of Fe^{2+}/Fe^{3+} in the samples as previously reported.[29] The ground state of Fe^{2+} exhibits temperature independent Van Vleck type paramagnetism that, in the present case, may produce changes in the measured diamagnetic contribution. However, no such changes have been observed, which indicate no relevant concentration of Fe ions in the 2+ charge state in the studied samples. Results in Table I show clearly that the paramagnetic Fe^{3+} ions are the most populated for Fe2a and Fe2b samples. For Fe1 sample, we may conclude for a magnetic conversion from ferromagnetic to paramagnetic phase after thermal annealing.

Finally, the origin of the ferromagnetism for the postannealed samples has been investigated by zero field cooling (ZFC) and field cooling (FC) measurements of the magnetization at low fields over the temperature range of 2–300 K. The results are displayed in Figure 8. There, we may observe a clear irreversibility of the ZFC and FC conditions. While the FC curve increases steadily with decreasing temperature, the ZFC curve exhibits a maximum at $T_{max} = 9$ K and decreases towards low temperatures. Both FC and ZFC curves intersect at about 250 K. This behavior is typical of an ensemble of superparamagnetic particles[30] and the observed maximum in the ZFC may be associated to a blocking temperature T_B. For a conventional spin glass system, the FC trace should present a plateau below T_{max}. Similar overall features have been obtained for sample Fe2bA (not shown here). In that case, T_B is about 11 K. Another feature that claims for the existence of superparamagnetic particles in the postannealed samples is the drop of the coercivity close to T_B. The coercive field H_c is found to be unchanged for T in the range 30–300 K with $H_c = 70$ Oe. Below 30 K, we may note a significant increase of H_c reaching 130 Oe at 10 K and 450 Oe at 1.7 K (Figure 7).

The results indicate also the existence of a second ferromagnetic phase with nonzero coercitivity for T above T_B.

The observed superparamagnetism is attributed to the formation of Fe based clusters (for example, α–Fe or Fe_xN) by annealing the Fe implanted samples. Such clusters have been also obtained in the previous work.[31] The presence of Fe clusters was not observed by Raman or XRD measurements, indicating that the size of these clusters is out of the detection limits.

IV. CONCLUSION

In summary, Fe has been successfully doped into high quality zincblende GaN epitaxial layers. Ferromagnetic behavior is observed for the as-implanted layers that is consistent with results for wurtzite Fe implanted GaN.[3,4] Our results show that both implantation dose and thermal treatment influence the magnetic properties of the studied samples. Dispersed Fe^{3+} ions coupled by a weak antiferromagnetic exchange interaction and characterized by a Curie-Weiss magnetic susceptibility are present in all studied samples. Thermal treatment is essential to remove the damage caused by the implantation. However, at the same time, it may contribute to the activation of Fe clustering for the high doses layers. On the other hand, the thermal treatment may redistribute the Fe ions in the GaN layer for the low dose sample. The Fe dispersion could explain the conversion from ferromagnetic to paramagnetic behavior observed after annealing.

Promising results in the study of the Fe implantation in cubic GaN have been obtained. Future work should focus on the improvement of the thermal treatment in order to obtain a compromise between structural quality of the layer and dilution of the implanted ions.

ACKNOWLEDGMENTS

[1] T. Dietl, H. Ohno, F. Matsukura, J. Cibert, and D. Ferrand, Science **287**, 1019–1022 (2000).
[2] A. Alsaad, Phys. B: Condens. Matter **440**, 1–9 (2014).
[3] N. Theodoropoulou, A. F. Hebard, S. N. G. Chu, M. E. Overberg, C. R. Abernathy, S. J. Pearton, R. G. Wilson, and J. M. Zavada, Appl. Phys. Lett. **79**, 3452–3454 (2001).
[4] Y. Shon, Y. H. Kwon, Y. S. Park, Sh. U. Yuldashev, S. J. Lee, C. S. Park, K. J. Chung, S. J. Yoon, H. J. Kim, W. C. Lee, D. J. Fu, T. W. Kang, X. J. Fan, Y. J. Park, and H. T. Oh, J. Appl. Phys. **95**, 761–763 (2004).
[5] L. E. Ramos, J. Furthmüller, J. R. Leite, L. M. R. Scolfaro, and F. Bechstedt, Phys. Rev. B **68**, 085209 (2003).
[6] K. Lorenz, I. S. Roqan, N. Franco, K. P. O'Donnell, V. Darakchieva, E. Alves, C. Trager-Cowan, R. W. Martin, D. J. As, and M. Panfilova, J. Appl. Phys. **105**, 113507 (2009).
[7] V. A. Chitta, J. A. H. Coaquira, J. R. L. Fernandez, C. A. Duarte, J. R. Leite, D. Schikora, D. J. As, K. Lischka, and E. Abramof, Appl. Phys. Lett. **85**, 3777–3779 (2004).
[8] F.-Y. Lo, A. Melnikov, D. Reuter, A. D. Wieck, V. Ney, T. Kammermeier, A. Ney, J. Schörmann, S. Potthast, D. J. As, and K. Lischka, Appl. Phys. Lett. **90**, 262505 (2007).
[9] J. Schörmann, S. Potthast, D. J. As, and K. Lischka, Appl. Phys. Lett. **90**, 041918 (2007).
[10] J. Ziegler, J. Biersack, and M. Ziegler, *SRIM—The Stopping and Range of Ions in Matter* (Lulu Books, 2008).
[11] J. P. Biersack and L. G. Haggmark, Nucl. Instrum. Methods **174**, 257–269 (1980).
[12] O. Madelung, U. Roessler, and M. Schulz, eds., "Silicon carbide (SiC), magnetic properties," *Landolt-Boernstein—Group III Condensed Matter* (Springer, Berlin, Heidelberg, 2002), Vol. 41A1b.
[13] D. P. Xu, Y. T. Wang, H. Yang, S. F. Li, D. G. Zhao, Y. Fu, S. M. Zhang, R. H. Wu, Q. J. Jia, W. L. Zheng, and X. M. Jiang, J. Appl. Phys. **88**, 3762–3764 (2000).
[14] X. H. Zheng, Y. T. Wang, Z. H. Feng, H. Yang, H. Chen, J. M. Zhou, and J. W. Liang, J. Cryst. Growth **250**, 345–348 (2003).
[15] S. Strite, J. Ruan, Z. Li, A. Salvador, H. Chen, D. J. Smith, W. J. Choyke, and H. Morkoç, J. Vac. Sci. Technol., B **9**, 1924–1929 (1991).
[16] B. Daudin, G. Feuillet, J. Hübner, Y. Samson, F. Widmann, A. Philippe, C. Bru-Chevallier, G. Guillot, E. Bustarret, G. Bentoumi, and A. Deneuville, J. Appl. Phys. **84**, 2295–2300 (1998).
[17] C. H. Wei, Z. Y. Xie, L. Y. Li, Q. M. Yu, and J. H. Edgar, J. Electron. Mater. **29**, 317–321 (2000).
[18] M. Häberlen, J. W. Gerlach, B. Murphy, J. K. N. Lindner, and B. Stritzker, J. Cryst. Growth **312**, 762–769 (2010).
[19] M. Leszcynski, I. Grzegory, and M. Bockowski, J. Cryst. Growth **126**, 601–604 (1993).
[20] B. E. Warren, *X-ray Diffraction*, Addison-Wesley Series in Metallurgy and Materials (Dover Publications, Inc., New York, 1990).
[21] R. C. Powell, N.-E. Lee, Y.-W. Kim, and J. E. Greene, J. Appl. Phys. **73**, 189–204 (1993).
[22] H. Liu, A. C. Frenkel, J. G. Kim, and R. M. Park, J. Appl. Phys. **74**, 6124–6127 (1993).
[23] H. Okumura, K. Ohta, G. Feuillet, K. Balakrishnan, S. Chichibu, H. Hamaguchi, P. Hacke, and S. Yoshida, J. Cryst. Growth **178**, 113–133 (1997).
[24] C. Liu, E. Alves, A. D. Sequeira, N. Franco, M. F. da Silva, and J. C. Soares, J. Appl. Phys. **90**, 81–86 (2001).
[25] M. Mamor, V. Matias, A. Vantomme, A. Colder, P. Marie, and P. Ruterana, Appl. Phys. Lett. **85**, 2244–2246 (2004).
[26] P. Wu, G. Saraf, Y. Lu, D. H. Hill, R. Gateau, L. Wielunski, R. A. Bartynski, D. A. Arena, J. Dvorak, A. Moodenbaugh, T. Siegrist, J. A. Raley, and Y. K. Yeo, Appl. Phys. Lett. **89**, 012508 (2006).
[27] A. Tabata, A. P. Lima, J. R. Leite, V. Lemos, D. Schikora, B. Schöttker, U. Köhler, D. J. As, and K. Lischka, Semicond. Sci. Technol. **14**, 318–322 (1999).
[28] D. G. Pacheco-Salazar, S. F. Li, F. Cerdeira, E. A. Meneses, J. R. Leite, L. M. R. Scolfaro, D. J. As, and K. Lischka, J. Cryst. Growth **284**, 379–387 (2005).
[29] A. Bonanni, M. Kiecana, C. Simbrunner, T. Li, M. Sawicki, M. Wegscheider, M. Quast, H. Przybylińska, A. Navarro-Quezada, R. Jakiela, A. Wolos, W. Jantsch, and T. Dietl, Phys. Rev. B **75**, 125210 (2007).
[30] O. Margeat, M. Respaud, C. Amiens, P. Lecante, and B. Chaudret, Beilstein J. Nanotechnol. **1**, 108–118 (2010).
[31] G. Talut, H. Reuther, S. Zhou, K. Potzger, F. Eichhorn, and F. Stromberg, J. Appl. Phys. **102**, 083909 (2007).